Time Series Graphical Lasso and Sparse VAR Estimation

Aramayis Dallakyan   Rakheon Kim   Mohsen Pourahmadi

Texas A&M University

Abstract

We improve upon the two-stage sparse vector autoregression (sVAR) method in Davis et al. (2016) by proposing an alternative two-stage modified sVAR method which relies on time series graphical lasso to estimate sparse inverse spectral density in the first stage, and the second stage refines non-zero entries of the AR coefficient matrices using a false discovery rate (FDR) procedure. Our method has the advantage of avoiding the inversion of the spectral density matrix but has to deal with optimization over Hermitian matrices with complex-valued entries. It significantly improves the computational time with a little loss in forecasting performance. We study the properties of our proposed method and compare the performance of the two methods using simulated and a real macro-economic dataset. Our simulation results show that the proposed modification or msVAR is a preferred choice when the goal is to learn the structure of the AR coefficient matrices while sVAR outperforms msVAR when the ultimate task is forecasting.

Keywords: Time Series Graphical Models, Sparse Vector Autoregression, FDR.

1   Introduction

A vector autoregressive (VAR) model is a powerful tool for analyzing multivariate time series. The recent increase in the availability of time series data pivots the interest of researchers toward high-dimensional VAR models. A common strategy in high-dimensional VAR estimation is to impose regularization on AR coefficient matrices. These methods can be grouped into three different approaches: regularized least square estimators using Lasso-type penalties (Song and Bickel, 2011; Basu and Michailidis, 2015; Kock and Callot, 2015; Nicholson et al., 2016; Barigozzi and Brownlees, 2019; Safikhani and Shojaie, 2020); regularized maximum-likelihood estimators (Basu and Michailidis, 2015; Davis et al., 2016; Yuen et al., 2018), and regularized Yule-Walker estimators using the CLIME or Dantzig estimators (Han et al., 2015; Wu and Wu, 2016; Ding et al., 2017).

Regularized least square VAR methods ignore the contemporaneous dependence in the time series since the loss function does not include the covariance of error terms. Song and Bickel (2011) discuss the possible impact in fitting a VAR model in which the contemporaneous dependence is ignored. Davis et al. (2016) numerically show that the forecasting performance of the VAR model improves when the information on the error covariance matrix is incorporated in the regularized log-likelihood. They proposed a two-stage approach to fit sparse VAR models. In the first stage, instead of working in a time domain, authors resort to a frequency domain and estimate the partial spectral coherence (PSC) to identify possible non-zero autoregressive coefficients (see Section 2.1 for details). Then, using constrained maximum likelihood estimation, parameters are estimated under the sparsity constraint. The lag order p and the number of pairs of non-zero AR parameters M are chosen using the Bayesian Information Criterion (BIC) over the specified grid values of M and p. In the second stage, the selected model is refined by identifying spurious non-zero AR coefficients. In particular, for non-zero AR coefficients, a sequence of t-statistics is created, and m of them are chosen using the BIC. The rest of the coefficients are considered spurious

and shrunk to zero. It is informative to note that the link between zero PSCs and zero AR coefficients is not exact. We give more details on this relationship in Appendix A.1.

In this paper, we improve the Davis et al. (2016) framework, by proposing a modification of their two-stage sVAR method, calling it modified sVAR (msVAR), with the following two key distinctions:

1. In msVAR, zeros of PSC are identified by employing time series graphical lasso (TS-Glasso) (Jung et al., 2015; Foti et al., 2016; Tugnait, 2018) to estimate the inverse spectral density matrix. The main advantage of such modification is to avoid inversion of a possibly high-dimensional matrix. However, TSGlasso involves optimization over Hermitian matrices with complex-valued entries which needs a special treatment, see Appendix B.

2. We use FDR in the refinement stage. The impetus of the FDR utilization is to substitute many pairwise hypothesis tests with a multiple hypothesis testing, which provides a better model selection framework (Benjamini and Gavrilov, 2009; Barber and Candès, 2015). In Section 5.1.5, our simulation results show the advantages of the FDR refinement in the second stage.

The remainder of the paper is organized as follows. Section 2 introduces details on the multivariate time series analysis, VAR, and the two-stage sVAR method. Time series graphical models and TSGlasso are discussed in Section 3, where TSGlasso requires tuning parameter selection to control sparseness and similarity of undirected graphs corresponding to the inverse spectral density matrices across the Fourier frequencies. Section 4 provides details of our algorithm for msVAR. In Section 5, we study and compare sVAR and msVAR using simulated and a real datasets. For the real data, in addition to sVAR and msVAR models, we consider Bayesian Ridge Regression VAR (BRRVAR) (Banbura et al., 2010), VAR with Lasso (LASSOVAR) penalty (Song and Bickel, 2011), and VAR with hierarchical componentwise (HVARC) and Own/Other (HVAROO) (Nicholson et al., 2016) penalties. Finally, we conclude with the discussion in Section 6.

2 Multivariate Stationary VAR Models

In this section, we review some basic properties of multivariate stationary processes, their spectral density matrices, VAR, and sVAR models.

2.1 Partial Spectral Coherence

In this part, we give a brief introduction to the PSC estimation. A deeper treatment can be found in Brillinger (1981); Brockwell and Davis (1986). Let $\{Y_{t,i}\}$ and $\{Y_{t,j}\}$ be two distinct marginal series of a K-variate stationary process $\{Y_t\}$, and $\{Y_{t,-ij}\}$ denotes the remaining $(K-2)$ marginal processes. The conditional correlation between two time series is computed by adjusting for the linear effect of the remaining marginal series $\{Y_{t,-ij}\}$. The linear effect of $\{Y_{t,-ij}\}$ is removed from the $\{Y_{t,i}\}$ by determining the optimal filter $\{D_{k,j}\}$ (Dahlhaus, 2000), which minimizes $E(Y_{t,i} - \sum_{k=-\infty}^{\infty} D_{ki} Y_{t-k,-ij})^2$. Then, the residual after removing the linear filter is:

$$\epsilon_{t,i} := Y_{t,i} - \sum_{k=-\infty}^{\infty} D_{k,i} Y_{t-k,-ij}. \tag{1}$$

The residual $\epsilon_{t,j}$ after removing the linear effect from $Y_{t,j}$ can be estimated similarly. Thus, two marginal series $\{Y_{t,i}\}$ and $\{Y_{t,j}\}$ are conditionally uncorrelated, if and only if their residual series $\{\epsilon_{t,i}\}$ and $\{\epsilon_{t,j}\}$ are uncorrelated at all lags; i.e., $\mathrm{cor}(\epsilon_{t+k,i}, \epsilon_{t,j}) = 0$ for all $k \in \mathbb{Z}$. In the frequency domain, $\{\epsilon_{t,i}\}$ and $\{\epsilon_{t,j}\}$ series being uncorrelated at all lags is equivalent to the cross-spectral density of two residual series being zero at all normalized frequencies $\omega \in [0,1]$, and the residual (cross)spectral density is defined as the Fourier transform of the autocovariance sequence

$$f_{ij}^{\epsilon}(\omega) := \frac{1}{2\pi} \sum_{k=-\infty}^{\infty} c_{ij}(k)^{\epsilon} e^{(-i2\pi k\omega)}, \ \omega \in [0,1], \tag{2}$$

where $c_{ij}(k)^{\epsilon} = cov(\epsilon_{t+k,i}, \epsilon_{t,j})$ is the (cross)autocovariance function of two marginal processes

4

in which we tacitly assume $\sum |c_{ij}(k)| < \infty$. The PSC between two distinct marginal series (Brillinger, 1981; Brockwell and Davis, 1986) is defined as:

$$PSC_{ij}(\omega) := \frac{f_{ij}^{\epsilon}(\omega)}{\sqrt{f_{ii}^{\epsilon}(\omega) f_{jj}^{\epsilon}(\omega)}}, \ \omega \in [0, 1]. \tag{3}$$

The residual cross-spectral density $f_{ij}^{\epsilon}(\omega)$ can be computed from the spectral density $f^Y(\omega)$ of the process $\{Y_t\}$ by

$$f_{ij}^{\epsilon}(\omega) = f_{ij}^{Y}(\omega) - f_{i,-ij}^{Y}(\omega)(f_{-ij,-ij}^{Y}(\omega))^{-1} f_{-ij,j}^{Y}(\omega), \tag{4}$$

where $f_{i,-ij}^{Y}$, $f_{-ij,-ij}^{Y}$ and $f_{-ij,j}^{Y}$ are some partitions of the spectral density matrix. (4) involves inverting $(K-2) \times (K-2)$ matrices $f_{-ij,-ij}^{Y}(\omega)$ for $\binom{K}{2}$ pairs, which is computationally challenging for high dimensional data. Dahlhaus (2000) proposed an efficient method to simultaneously compute PSC for all $\binom{K}{2}$ pairs by inverting the $K \times K$ spectral density matrix. Thus, setting $\Theta^Y(\omega) := f_{ij}^{Y}(\omega)^{-1}$, the PSC can be computed as follows:

$$PSC_{ij}(\omega) = -\frac{\Theta_{ij}^{Y}(\omega)}{\sqrt{\Theta_{ii}^{Y}(\omega) \Theta_{jj}^{Y}(\omega)}}, \tag{5}$$

where $\Theta_{ii}^{Y}(\omega)$, $\Theta_{jj}^{Y}(\omega)$ are the ith and jth diagonal entries and $\Theta_{ij}^{Y}(\omega)$ the (i, j)th entry of $\Theta^Y(\omega)$. From (2),(3) and (5), it can be seen that $\{Y_{t,i}\}$ and $\{Y_{t,j}\}$ are conditionally uncorrelated iff $\Theta_{ij}^{Y}(\omega) = 0$ for all $\omega \in [0, 1]$. Note that PSC and the inverse spectral density matrix are analogs of familiar notions of partial correlations and inverse covariance matrices in multivariate statistics.

2.2 VAR and sVAR Models

Consider K dimensional VAR model of order p (VAR(p)):

$$Y_t = a + A_1 Y_{t-1} + \cdots + A_p Y_{t-p} + u_t, \tag{6}$$

where $Y_t = (y_{1t}, \ldots, y_{Kt})^T$ is a random vector, A_i's are fixed $(K \times K)$ coefficient matrices, and $a = (a_1, \ldots, a_K)^T$ is a $(K \times 1)$ vector of intercept. The K-dimensional white noise is given by $u_t = (u_{1t}, \ldots, u_{Kt})^T$ where $E(u_t) = 0$, $E(u_t u_s^T) = \Sigma_u$ for $t = s$, and $E(u_t u_s^T) = 0$ otherwise. We further assume that the process is stable, i.e., $\det(I_k - \sum_{i=1}^{p} A_i z^i) \neq 0$ for $z \in \mathcal{C}$, $|z| \leq 1$.

Given time series observations $Y_1, \ldots, Y_T$, fitting VAR models amounts to estimating the lag order p and the coefficient matrices $A_1, \ldots, A_p$. However, when K is large or even moderate, the VAR model is over-parametrized since the number of parameters grows quadratically $(K^2 p)$. Therefore, there is growing interest in developing sparse methods to overcome the computational problem and the interpretation of the model parameters, see for example Song and Bickel (2011); Davis et al. (2016); Nicholson et al. (2016); Ding et al. (2017); Yuen et al. (2018); Safikhani and Shojaie (2020).

2.2.1 Two-stage sVAR

In this section, we describe the two-stage sVAR approach introduced in Davis et al. (2016). Algorithm 1 reports Stage 1 and 2 of the sVAR algorithm.

Stage 1: Model Selection: The first stage exploits PSC to set to zero certain entries of coefficient matrices. More precisely,

$$PSC_{ij}(\omega) = 0, \ \omega \in [0,1] \implies A_k(i,j) = A_k(j,i) = 0, \ k = 1, \ldots, p. \tag{8}$$

Algorithm 1: sVAR algorithm

Stage 1

1. Invert estimated spectral density matrix and compute the PSC for all $K(K-1)/2$ pairs of distinct marginal series.
2. Construct a sequence Q_1 by ranking summary statistics $\mathcal{S}_{ij}$'s (see (9)) from highest to lowest.
3. For each $(p, M) \in \mathbb{P} \times \mathbb{M}$, set the order of autoregression to p and feed the top M pairs in the sequence Q_1 to the VAR model. Estimate parameters under this constraint and compute the corresponding $BIC(p, M)$:

$$BIC(p, M) = -2 \log L(A_1, \ldots, A_p) + \log T \cdot (K + 2M)p \qquad (7)$$

4. Choosethe number of lags and non-zero pairs (p^*, M^*) that gives the minimum BIC value over $\mathbb{P} \times \mathbb{M}$

Stage 2

1. For each of the non-zero AR coefficient compute the t-statistic via (10),
2. Construct the sequence Q_2 of the $(K + 2M^*)p^*$ triplets (i, j, k) by ranking $|t_{i,j,k}|$ from highest to lowest,
3. For each $m \in \{0, 1, \ldots, (K + 2M^*)p^*\}$ select the m non-zero AR coefficient corresponding to the top triplets in the sequence Q_2 and compute $BIC(m) = -2 \log L + \log T \cdot m$,
4. Choose the number of non-zero m^* that gives the minimum BIC value: $BIC(m^*) = -2 \log L + \log T \cdot m^*$.

As discussed, this relationship is only an assertion and is not exact for some cases. See Section A.1 for more details.

Thus, a group of AR coefficient estimates is set to zero if the corresponding PSC estimates are zero. However, because of the sampling variability, estimated PSCs are not exactly zero even though two marginal series are conditionally uncorrelated. Davis et al. (2016) overcome this problem by ranking estimated PSCs from largest to smallest and finding a threshold that separates non-zero PSCs in which the supremum of the squared modulus of the estimated PSC is used as summary statistics:

$$\mathcal{S}_{ij} := \sup |PSC_{ij}(\omega)|^2, \qquad (9)$$

where the supremum is taken over all scaled frequencies ω. Thus, a large value of $\mathcal{S}_{ij}$ indicates that two marginal series are conditionally correlated and vice versa.

The output of the first stage algorithm is a model with $(K + 2M^*)p^*$ non-zero AR coefficients. If the proportion of selected pairs is small, then the number of non-zero parameters is much smaller than that for the fully-parametrized VAR(p^*), where the number of parameters is $K^2 p^*$. In Step 3, the parameter estimation under the constraint is implemented using constrained log-likelihood estimation described in Lütkepohl (2007, Chapter 5).

Stage 2: Refinement: In Stage 1, the PSC can only be evaluated for pairs of series, but it does not consider diagonal entries in $A_1, \ldots, A_p$ and within the group coefficients for each pair of component series. In other words, Stage 1 may produce spurious non-zero AR coefficients. To emancipate the model from spurious coefficients, in the $(K + 2M^*)p^*$ sequence of non-zero AR coefficients, Davis et al. (2016) rank them according to the absolute value of their t-statistics, i.e.,

$$t_{i,j,k} := \frac{A_k(i, j)}{se(A_k(i, j))}, \tag{10}$$

where the standard error $se(A_k(i, j))$ is computed from the asymptotic distribution of the constrained maximum likelihood estimator (Lütkepohl, 2007). After the second stage, the procedure leads to a sparse VAR model that contains m^* non-zero AR coefficients, denoted by sVAR(p^*, m^*).

3 Time Series Graphical Lasso

The salient feature of Gaussian graphical models is to represent conditional independencies among random variables in multivariate data. An undirected graph is a powerful tool for visualizing these relationships where the vertices represent the random variables, and the edge between two vertices indicates the conditional dependence of corresponding variables. For a K-dimensional random vector $Y \sim N_K(0, \Sigma)$, a Gaussian graphical model

can be constructed from the inverse covariance matrix $\Theta = \Sigma^{-1}$. More precisely, a zero off-diagonal entry of $\Theta_{ij} = 0$ implies that Y_i and Y_j are conditionally independent given all other variables (Whittaker, 1990). When K is large, it is reasonable to impose structure or regularize Θ directly in the search for sparsity (Banerjee et al., 2008; Friedman et al., 2008), see Pourahmadi (2013) for an overview.

Given the sample data, a regularized Gaussian graphical model estimation can be formulated as

$$\min_{\Theta} \log \det(\Theta) - \mathrm{tr}(S\Theta) + P(\Theta, \lambda), \tag{11}$$

where $\det(\cdot)$ is determinant of the matrix, S is the sample covariance matrix, $P(\cdot)$ is a penalization term, and λ is a tuning parameter. In Banerjee et al. (2008); Friedman et al. (2008) the penalization term is ℓ_1 norm, i.e., $P(\Theta, \lambda) = \lambda \|\Theta\|_1 = \lambda \sum_{ij} |\theta_{ij}|$. The Glasso algorithm is extremely popular and has been extended to multiple covariance matrices in Guo et al. (2011); Danaher et al. (2014) where the data from several populations may have a similar graphical structure.

Brillinger (1996) and Dahlhaus (2000) have extended the use of graphical models to the multivariate time series setup. Consider K dimensional stationary process Y_t, $t = 1, \ldots, T$. Let $G = (V, E)$ denote a graph, where each node $v \in V$ corresponds to one of the times series in Y_t and the edge between nodes is characterized by the conditional dependence of the marginal series Y_i and Y_j, given the rest Y_{-ij}; i.e., $Y_i - Y_j$ iff $\Theta_{ij}^Y(\omega) = 0$, or $\mathrm{PSC}(\omega) = 0$ for $\omega \in [0, 1]$. From now on, whenever there is no confusion in the context, we drop the superscript Y from Θ, and note that $\Theta(\cdot)$ is a Hermitian matrix-valued function with complex-valued entries.

A time series extension of the Glasso requires expressing the log-likelihood function in terms of the discrete Fourier transform of the data and $\Theta(\cdot)$. Define the normalized discrete

Fourier transform (DFT) of K dimensional random vector Y_t,

$$d(\omega_n) = \frac{1}{\sqrt{T}} \sum_{t=0}^{T-1} Y_t \exp(-i2\pi\omega_n t), \tag{12}$$

where $i = \sqrt{-1}$, $\omega_n = n/T$, $n = 0, 1, \ldots, T-1$. Since Y_t is real-valued, the complex conjugate $d^*(\omega_n) = d(-\omega_n) = d(1-\omega_n)$ and for $n = 0, 1, \ldots, T/2$, $d(\omega_n)$ is completely determined for all n. Moreover, from Brillinger (1981, Theorem 4.4.1) as $T \to \infty$, $d(\omega_n)$, $n = 1, 2, \ldots, (T/2)-1$ are independent complex Gaussian $N_c(0, f[\omega_n])$ random vectors and for $n = \{0, T/2\}$, $d(\omega_n)$ are independent real Gaussian $N_r(0, f[\omega_n])$. Ignoring $n = \{0, T/2\}$ frequency points, and denoting $f[\omega_n] = f[n]$, $\Theta[n] = f^{-1}[n]$, the joint pdf for $d(\omega_n)$, $n = 1, \ldots, (T/2) - 1$ is

$$g(d(\omega_1), \ldots, d(\omega_{(T/2)-1})) = \prod_{n=1}^{(T/2)-1} \frac{\exp(-d^H(\omega_n)\Theta[n]d(\omega_n))}{\pi^K \det(f[n])} \tag{13}$$

A standard assumption in spectral density estimation is locally smoothness (Brillinger, 1981; Stoica and Moses, 1997), i.e., $f[n]$ is approximately constant over $L = 2m_t + 1 \geq K$ consecutive frequency points where m_t is the half-window size. After carefully picking

$$\tilde{\omega}_l = \frac{(l-1)L + m_t + 1}{T}; \; M = \left\lfloor \frac{T/2 - m_t - 1}{L} \right\rfloor; \; l = 1, 2, \ldots M,$$

leads to M equally spaced frequencies $\tilde{\omega}_l$. Therefore, the exploitation of the local smoothness assumption results for $k = -m_t, -m_t + 1, \ldots, m_t$

$$\tilde{\omega}_{l,k} = \frac{(l-1)L + m_t + 1 + k}{T}; \; f[k] = f[\{l, k\}]. \tag{14}$$

From (14) and (13), the pdf is

$$g(d(\omega_1), \ldots, d(\omega_{(T/2)-1})) = \prod_{n=1}^{M} \prod_{l=-m_t}^{m_t} \frac{\exp(-d^H(\tilde{\omega}_{l,n})\Theta[n]d(\omega_{l,n}))}{\pi^K \det(f[n])^L}$$

$$= \prod_{l=1}^{M} \frac{\exp[-\mathrm{tr}(\tilde{f}[n]\Theta[n])]}{\pi^{LK} \log \det f[n]},$$

(15)

where $\tilde{f}[n] = \sum_{l=-m_t}^{m_t} d(\tilde{\omega}_{l,n})d^H(\tilde{\omega}_{l,n})/L$ is the sample spectral density matrix whose entries are potentially complex-valued. Thus, the log-likelihood function can be written as

$$W(\Theta[\cdot]) = \sum_{n=1}^{M} L \left[\log \det(\Theta[n]) - \mathrm{tr}(\tilde{f}[n]\Theta[n]) \right].$$

Analogous to Glasso, we introduce sparsity by minimizing the following regularized log-likelihood

$$\min_{\Theta[n]} W(\Theta[\cdot]) + P(\Theta[\cdot], \lambda),$$

(16)

where

$$P(\Theta[\cdot], \lambda) = \lambda \sum_{i \neq j} \sqrt{\sum_{n=1}^{N} |\Theta_{ij}[n]|^2}, \ \Theta[\cdot] = \{\Theta[1], \ldots, \Theta[N]\},$$

(17)

As in Jung et al. (2015), we appeal to the alternating direction method of multipliers (ADMM) (Boyd et al., 2011) for minimization. However, in the following we pay due attention to the fact that the entries of Θ are complex-valued. The ADMM minimizes the scaled augmented Lagrangian

$$L_\rho(\Theta[\cdot], Z[\cdot], U[\cdot]) = \sum_{n=1}^{M} L \left[-\log \det(\Theta[n]) + \mathrm{tr}(\tilde{f}[n]\Theta[n])) \right] + \lambda P(Z[\cdot])$$

$$+ \rho/2 \sum_{n=1}^{M} \|\Theta[n] - Z[n] + U[n]\|_F^2,$$

(18)

subject to $\Theta[n] = Z[n]$ and $\|X[n]\|_F^2 = \sum_{ij} |X_{ij}[n]|^2$ for $n = 1, \ldots, M$. Given $(\Theta^{(k)}[\cdot], Z^{(k)}[\cdot], U^{(k)}[\cdot])$ matrices in the kth iteration, the ADMM algorithm implements the

following three updates for the next $(k+1)$ iteration:

(a) $\Theta^{(k+1)}[\cdot] \leftarrow \arg\min_{\Theta[\cdot]} L_\rho(\Theta[\cdot], Z^{(k)}[\cdot], U^{(k)}[\cdot])$

(b) $Z^{(k+1)}[\cdot] \leftarrow \arg\min_{Z[\cdot]} L_\rho(\Theta^{(k+1)}[\cdot], Z[\cdot], U^{(k)}[\cdot])$

(c) $U^{(k+1)}[\cdot] \leftarrow U^{(k)}[\cdot] + (\Theta^{(k+1)}[\cdot] - Z^{(k+1)}[\cdot])$

It is timely and instructive to note that unlike the formulation in (11) (Banerjee et al., 2008; Friedman et al., 2008; Danaher et al., 2014) where Θ is real-valued, here we have to deal with a complex-valued $\Theta[\cdot]$ in (18). While Li et al. (2015) establish steps for the complex-valued ADMM when the penalty function is ℓ_1 norm, here we resort to Wirtinger calculus (Wirtinger, 1927; Brandwood, 1983), coupled with the definition of Wirtinger subgradients (Bouboulis et al., 2012), to derive updates (a)-(c) for matrices with complex entries. Details are relegated to Appendix B.

Boyd et al. (2011, Section 3.1) showed that for a given ρ, the convergence of iterates to the global minimum is guaranteed. The choice of ρ controls the speed of convergence. Boyd et al. (2011, Section 3.4.1) discuss the adaptive choice of ρ to improve convergence. On the statistical side, Jung et al. (2015) provide an upper bound on the support recovery of the TSGlasso.

3.1 Tuning Parameter Selection for TSGlasso

In the TSGlasso algorithm, the tuning parameter λ controls the sparsity and the similarity of the estimated undirected graphs over the scaled frequencies. In this section, we review some classical methods for tuning parameter selection.

Ideally, the selected tuning parameter should produce an undirected graph that is sufficiently complex to be interesting, sufficiently sparse to be interpretable, and, more importantly, should be supported by data. The traditional approaches such as the Akaike information criterion (AIC), Bayesian information criterion (BIC) and cross-validation tend

to choose graph that is too large (Meinshausen and Bühlmann, 2010). Homrighausen and McDonald (2018) empirically showed that for the penalized regression, the tuning parameter, selected from the Stein unbiased risk estimator (SURE)-type criterion, tends to perform better than other considered criteria. For graphical models, extended BIC, introduced in Foygel and Drton (2010), shows practical superiority compare to discussed criteria.

From (15), the AIC approximation for the time series graphical model is:

$$\text{AIC}(\lambda) = \sum_{n=1}^{M} \Big[-\log \det \hat{\Theta}_\lambda[n] + \text{tr}(\tilde{f}(n)\hat{\Theta}_\lambda[n]) \Big] \times L + 2E_n, \tag{19}$$

where $\hat{\Theta}_\lambda[n]$ is the estimated inverse spectral density at tuning parameter λ, and E_n is the number of non-zero elements in $\hat{\Theta}_\lambda[n]$. Using AIC, we choose λ which gives the minimum value of (19). Similarly, an approximation of the extended BIC is:

$$\text{eBIC}(\lambda) = \sum_{n=1}^{M} \Big[-\log |\hat{\Theta}_\lambda[n]| + tr(\tilde{f}[n]\hat{\Theta}_\lambda[n]) \Big] \times L + \log(L)E_n + 4E_n\gamma \log(K), \tag{20}$$

with a hyper-parameter $\gamma \in [0,1]$. If $\gamma = 0$, then (20) reduces to the classical BIC. The higher value of γ leads to the stronger penalization of large graphs. For the moderate and large values of K, Foygel and Drton (2010) suggest $\gamma = 0.5$.

4 Modified sVAR

In this section, we introduce our msVAR procedure and highlight the key differences with the sVAR. Algorithm 2 summarizes the proposed modifications.

The first stage of our Algorithm is designed to avoid the costly matrix inversion and grid search procedure to compute constrained MLE of the AR parameters. We substitute Steps 1 - 3 of the sVAR's Stage 1 (see Algorithm 1) by the TSGlasso algorithm, with the ensuing M^* non-zero elements, and use BIC only once to choose the number of lags p^* compare to

Algorithm 2: msVAR algorithm

Stage 1

1. Estimate the inverse spectral density matrix using TSGlasso, and let M^* be its number of non-zero elements (see Section 3).
2. Estimate the AR parameters under the zero constraint and choose the number of lags (p^*) by minimizing

$$BIC(p) = -2 \log L(A_1, \ldots, A_p) + \log T(K + 2M^*)p$$

Stage 2

1. For each of the non-zero AR coefficient compute the t-statistic and p-value.
2. Choose m^* non-zero coefficients that reject hypothesis in FDR procedure with the threshold value of FDR-corrected significance q.

---

sVAR (see Step 3 in Stage 1 in Algorithm 1).

In the second stage, instead of using t-statistics of the AR coefficients, our algorithm relies on the FDR (Benjamini and Hochberg, 1995) procedure for further refinement. There is a rich literature on the use of FDR for model selection, for example, see Benjamini and Gavrilov (2009); Barber and Candès (2015); G'Sell et al. (2016), etc. The advantage of FDR utilization in the second stage is twofold: First, instead of pairwise t-statistics, we implement multiple hypothesis testing. Second, it eliminates the need for Step 3 in Stage two of sVAR (see Algorithm 1). The empirical analysis in Appendix 5.1.5 further shows the advantages of using FDR for refinement.

5   Numerical Results

In this section, we use simulated and real datasets to compare the performance of msVAR and sVAR models. Our analyses indicate that msVAR is a preferred choice when the goal is to learn the structure of the coefficient matrix. On the other hand, sVAR outperforms msVAR when the ultimate task is forecasting. The analysis in Section 5.1.4 shows that the proposed modifications significantly improve the computation time of the algorithm.

5.1 Comparing the msVAR and sVAR Models

5.1.1 Evaluation Measures and Visualization

The following metrics are computed to compare the performance of the two methods:

- the squared bias of the AR coefficient estimates:

$$\sum_{k=1}^{max(p,\hat{p})} \sum_{i,j=1}^{K} [\mathbb{E}[\hat{A}_k(i,j)] - A_k(i,j)]^2;$$

- the variance of the estimated AR coefficient:

$$\sum_{k=1}^{max(p,\hat{p})} \sum_{i,j=1}^{K} var(\hat{A}_k(i,j));$$

- the mean square error (MSE) of the AR coefficient estimates:

$$\sum_{k=1}^{max(p,\hat{p})} \sum_{i,j=1}^{K} \{[\mathbb{E}[\hat{A}_k(i,j)] - A_k(i,j)]^2 + var(\hat{A}_k(i,j))\}.$$

- the true positive rate (TPR): estimates the ratio between the number of correctly found edges in estimated graph and the number of true edges in the true graph.

- the false positive rate (FPR): estimates the ratio between the number of incorrectly found edges in estimated graph and the number of true missing edges in the true graph.

In addition, we utilize a Eichler (2012)'s proposal to visualize an estimated VAR model using a mixed graph. The edge set E_m of the mixed graph $G_m = (V_m, E_m)$ consists of directed and undirected edges, in which

- $i \rightarrow j \notin E_m$ whenever $A_k(i,j) = 0$, $k = 1, \ldots, p$
- $i{-}j \notin E_m$ whenever $(\Theta_u)_{ij} = (\Theta_u)_{ji} = 0$.

In other words, the directed edge is in the edge set whenever Y_i is Granger-causal for Y_j (Lütkepohl, 2007), and an undirected edge is in the edge set whenever Y_i and Y_j are

15

contemporaneously conditionally dependent. However, for the sake of clarity, we present only the directed part of the mixed graph as in Figures 1-3.

5.1.2 The Simulation Setup

In the simulation study, we consider three different *stable* VAR models to compare performance of sVAR and msVAR methods.

Model 1: $y_t = A_1 y_{t-1} + u_t$, and $K = 10$

$$
A_1 = \begin{bmatrix}
0 & 0 & 0 & 0 & 0 & 0 & 0 & 0.3 & 0 & 0 \\
0 & 0 & 0.1 & 0 & 0 & 0 & 0.4 & 0 & 0 & 0.4 \\
0 & 0.6 & 0 & 0 & 0 & 0 & 0 & 0 & 0 & 0 \\
0 & 0.2 & 0 & 0 & 0.5 & 0 & 0 & 0 & 0 & 0 \\
0 & 0.3 & 0 & 0.1 & 0 & 0 & 0.2 & 0.1 & 0.3 & 0.5 \\
0.2 & 0 & 0 & 0 & 0.4 & 0 & 0 & 0 & 0 & 0 \\
0 & 0 & 0 & 0 & 0 & 0 & 0 & 0 & 0 & 0.6 \\
0 & 0 & 0 & 0 & 0 & 0.6 & 0 & 0 & 0 & 0 \\
0.2 & 0 & 0 & 0 & 0 & 0 & 0 & 0 & 0.2 & 0 \\
0 & 0 & 0 & 0 & 0.4 & 0 & 0 & 0 & 0 & 0
\end{bmatrix}, \Theta_u = \begin{bmatrix}
\delta & \delta/2 & \cdots & \delta/10 \\
\delta/2 & 1 & \cdots & 0 \\
\vdots & \vdots & \ddots & 0 \\
\delta/10 & 0 & \cdots & 1
\end{bmatrix},
$$

where $\delta = 0.5$. The setup of the simulation is borrowed from the Davis et al. (2016, Section 4). See Figure 1 for illustration.

Model 2: $y_t = A_1 y_{t-1} + u_t$, and $K = 6$

$$
A_1 = \begin{bmatrix}
0 & 0.50 & 0.50 & 0.20 & 0 & 0 \\
0 & 0 & 0.30 & 0 & 0 & 0 \\
0 & 0.25 & 0.50 & 0 & 0 & 0 \\
0 & 0 & 0 & 0 & 0.33 & 0.33 \\
0 & 0 & 0 & 0 & 0 & 0.20 \\
0 & 0.50 & 0 & 0 & 0.17 & 0.33
\end{bmatrix}, \Theta_u = \begin{bmatrix}
0.17 & 0 & 0.25 & 0.030 & 0 & 0 \\
0 & 1.40 & 0.34 & 0.25 & 0.04 & 0.58 \\
0.25 & 0.34 & 0.55 & 0.05 & 0 & 0 \\
0.03 & 0.25 & 0.05 & 0.26 & 0 & 0.42 \\
0 & 0.04 & 0 & 0 & 1.51 & 0.36 \\
0 & 0.58 & 0 & 0.42 & 0.36 & 0.98
\end{bmatrix}
$$

The purpose of this setup is to compare methods when for some entries of A_1 the assertion (8) is violated

$$
\text{PSC}_{ij}(\omega) = 0, \ \omega \in [0, 1] \text{ and } A_1[i, j] \neq 0 \tag{21}
$$

See Figure 2 for illustration. Red directed edges indicate entries of A_1 that violate assertion (8).

Remark 1. *In general, for any element of A_1, enforcement of (21) is not a trivial task. Values and structure of coefficient matrices A_1 and Θ_u are carefully constructed such that $A_1[1,2]$ and $A_1[4,5]$ satisfy condition (22) located in the Appendix.*

Model 3: $y_t = A_1 y_{t-1} + A_2 y_{t-2} + u_t$, and $K = 6$

$$A_1 = \begin{bmatrix} -0.6 & 0.4 & 0 & 0 & 0 & 0.4 \\ 0.4 & -0.6 & 0.4 & 0 & 0 & 0 \\ 0 & 0.4 & -0.6 & 0.4 & 0 & 0 \\ 0 & 0 & 0.4 & -0.6 & 0.4 & 0 \\ 0 & 0 & 0 & 0.4 & -0.6 & 0.4 \\ 0.4 & 0 & 0 & 0 & 0.4 & -0.6 \end{bmatrix}, A_2 = \begin{bmatrix} -0.3 & 0.2 & 0 & 0 & 0 & 0.2 \\ 0.2 & -0.3 & 0.2 & 0 & 0 & 0 \\ 0 & 0.2 & -0.3 & 0.2 & 0 & 0 \\ 0 & 0 & 0.2 & -0.3 & 0.2 & 0 \\ 0 & 0 & 0 & 0.2 & -0.3 & 0.2 \\ 0.2 & 0 & 0 & 0 & 0.2 & -0.3 \end{bmatrix}$$

$$\Theta_u = \begin{bmatrix} 1 & -0.3 & 0 & 0 & 0 & -0.3 \\ -0.3 & 1 & -0.3 & 0 & 0 & 0 \\ 0 & -0.3 & 1 & -0.3 & 0 & 0 \\ 0 & 0 & -0.3 & 1 & -0.3 & 0 \\ 0 & 0 & 0 & -0.3 & 1 & -0.3 \\ -0.3 & 0 & 0 & 0 & -0.3 & 1 \end{bmatrix}$$

This setup is borrowed from Yuen et al. (2018, Section 4). The directed graph is illustrated in Figure 3.

For each model, the corresponding multivariate time series is generated following Lütkepohl (2007, Appendix D1) over the 50 replications. For all models, $T = 100$ and for the tuning parameter selection in Stage 1, we only report results for the eBIC since BIC and AIC provide similar outcomes. For Stage 2 of the msVAR, the threshold value of FDR-corrected significance is fixed at $q = 0.1$.

5.1.3 The Simulation Result

Figures 1 - 3 and Table 1 report the simulation results for Models 1 - 3, respectively. In each figure, top left directed graph corresponds to the true case and top right and bottom left to the msVAR and sVAR, respectively. The width and color shade of the estimated edges correspond to the proportion of times the edge was detected out of 50 replications; i.e., the darker and thicker the edge, more frequently it was present and vice versa. In Figure 2, red

17

directed edges correspond to the condition (21). In Table 1, for each method, the minimum of $Bias^2$, Variance, MSE and FPR metrics, and the maximum of TPR are highlighted.

From Figures 1 - 3, the visual comparison reveals that both msVAR and sVAR were able to detect true edges for most of the time. For Model 1, msVAR indicates better result on estimating true edges than sVAR. For example, sVAR failed to detect the edge $Y_5 \longleftrightarrow Y_{10}$ in all repetitions, while msVAR detected it around 90% of time. The first two rows in Table 1 document the five metrics comparison for Model 1. It can be seen, that msVAR is the best for all metrics.

A similar result holds for Model 2. msVAR shows small bias but higher variance and the best TPR result. More importantly, both algorithms were able to detect the edges $Y6 \longrightarrow Y2$ and $Y1 \longrightarrow Y2$ most of the time, even thought the assertion (8) was violated. For Model 3, the performance is reversed compared to Model 2, i.e., msVAR shows slightly higher bias but smaller variance.
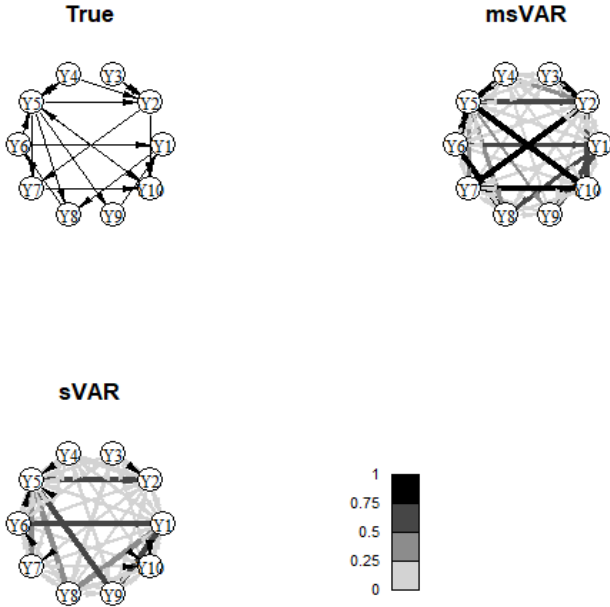

Figure 1: Model 1 simulation result. The width and color shade of estimated edges indicate the proportion of the number of times the edge was detected out of 50 replication.
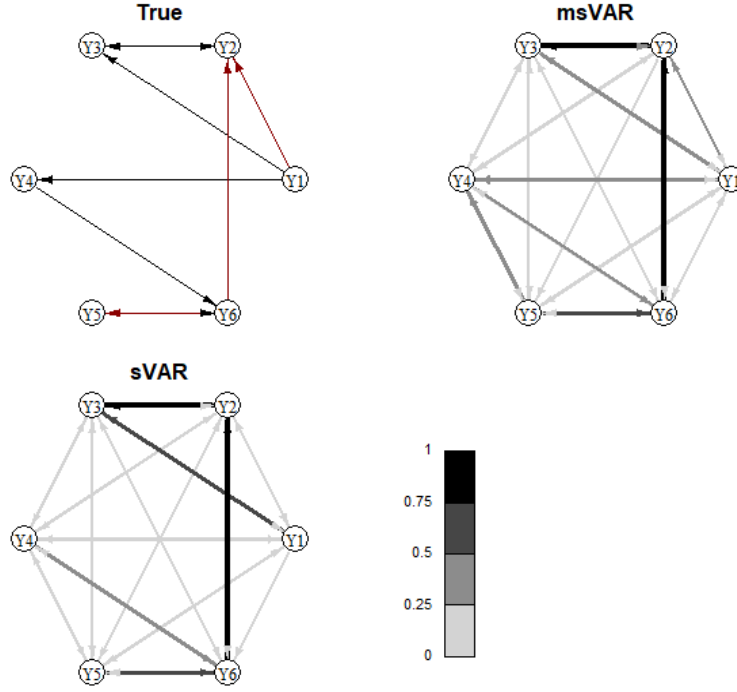
Figure 2: Model 2 simulation result. Red directed edges in the true graph correspond to the condition (21). The width and color shade of estimated edges indicate the proportion of the number of times the edge was detected out of 50 replication.
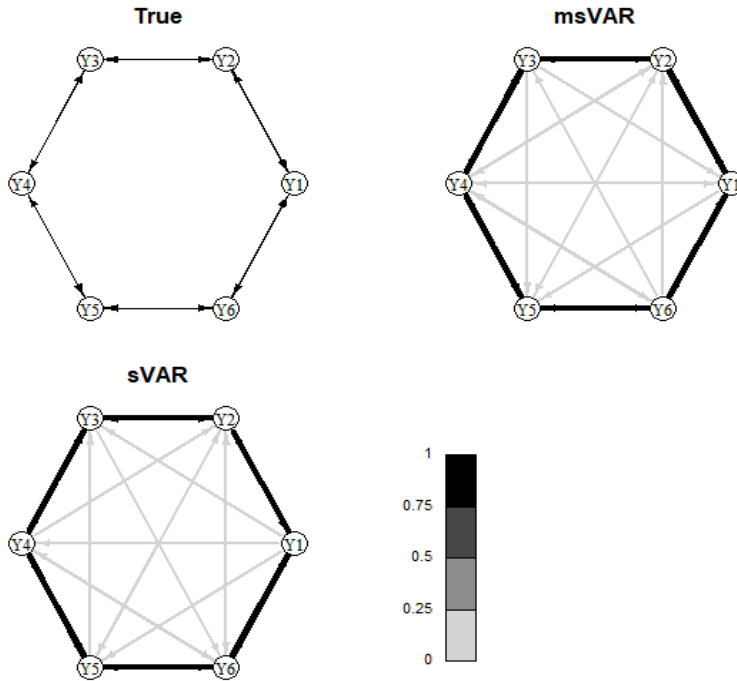

Figure 3: Model 3 simulation result. The width and color shade of estimated edges indicate the proportion of the number of times the edge was detected out of 50 repetition.

Table 1: Five metrics from the sVAR and msVAR methods.

	Method	Bias^2	Variance	MSE	TPR	FPR
Model 1	sVAR	0.178	0.788	0.966	0.595	0.03
	msVAR	**0.174**	**0.732**	**0.906**	**0.632**	**0.02**
Model 2	sVAR	0.508	**0.609**	**1.117**	0.477	**0.08**
	msVAR	**0.303**	0.951	1.254	**0.537**	0.118
Model 3	sVAR	**0.089**	0.762	0.851	**0.954**	**0.03**
	msVAR	0.102	**0.742**	**0.844**	0.946	0.05

5.1.4 Running Time Comparison

In this section, we compare relative running times for sVAR and msVAR methods. For this exercise, we fixed $p = 1$, and for $K = 15, 25, 50, 75$, generate a sparse coefficient matrix A such that the probability of having a non-zero element is equal to 0.25. Then, the coefficient matrix is rescaled to satisfy the stability condition. For the msVAR method, we select two options for time comparison: msVAR with tuning parameter selection and without, respectively. For brevity, we call those methods *msVAR with* and *msVAR without*. In the former case, the tuning parameter is selected over 20 equally spaced values located in $(0, 1)$ interval, and for the latter case, the tuning parameter is fixed to $\lambda = 0.2$. The relative time is reported with respect to the running time of the *msVAR without*. The modified R code for the msVAR algorithm relies on the sVAR code framework provided in Davis et al. (2016). Table 2 reports relative times for $K = 15, 25, 50, 75$.

Table 2: Relative running times for the sVAR and msVAR algorithm. Running times are reported relative to the msVAR algorithm.

K	msVAR with	msVAR without	sVAR
15	10.03	1	4.27
25	4.91	1	38.80
50	1.02	1	68.50
100	1.01	1	$-^*$

Note: * The algorithm was terminated after 24 hours.

It can be seen when $K = 15$, the *msVAR without* is the fastest, followed by the sVAR, which is nearly 4.3 times slower than the *msVAR without*. Finally, the *msVAR with* is almost 10 times slower than the *msVAR without*. However, sVAR becomes extremely slow as K grows. For large K, running times for the *msVAR without* and *msVAR with* are almost indistinguishable. The result can be explained by observing that in both methods, the computationally expensive procedure is the restricted MLE estimation, and msVAR is fast since it implements it once, compared to sVAR's grid search approach. Moreover, the computational expense of restricted MLE estimation overshadows the computation time of the tuning parameter selection as K grows.

5.1.5 Comparing msVAR stage 1 and stage 2 outputs

In this section, we compare msVAR stage 1 and stage 2 outputs. Recall that in stage 2 of msVAR, we use the FDR procedure for edge selection. For comparison, we use Model 1, described in Section 5, to generate the dataset. Table 3 and Figure 4 report the results. Results from both table and figure indicate the performance improvement after the FDR refinement in stage 2.

Table 3: Three metrics from the msVAR and msVAR St.1 methods.

	Bias^2	Variance	MSE
msVAR St.1	0.524	1.249	1.774
msVAR	**0.508**	**0.925**	**1.433**

5.2 Real Data Analysis

We compare the forecasting performance of various VAR methods on a real-world macro-economic dataset. In addition to sVAR and msVAR, we consider Bayesian Ridge Regression VAR (BRRVAR) (Banbura et al., 2010), VAR with Lasso (LASSOVAR) penalty (Song and Bickel, 2011), and VAR with hierarchical componentwise (HVARC) and Own/Other (HVA-
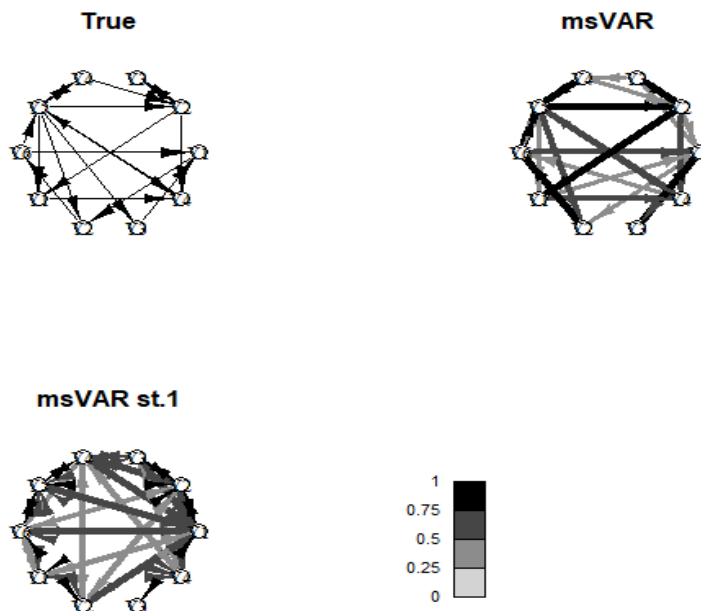
Figure 4: Model 1 simulation result. The width and color shade of estimated edges indicate the proportion of the number of times the edge was detected out of 50 replication.

ROO) (Nicholson et al., 2016) penalties. Corresponding tuning parameters for the LASSO-VAR, HVARC, and HVAROO are selected using rolling cross-validation (Nicholson et al., 2016).

The dataset represents the 168 monthly US macro-economic time series from 01/1959 to 02/2009. Initially, the dataset was compiled by Stock and Watson (2005) and latter augmented by Koop (2011). Koop (2011) defines and analyzes a small (K = 3), medium (K = 20), medium-large (K = 40) and large (K = 168) VARs. In this paper, we focus only on the medium-large setup with $K = 40$ variables. To avoid a policy break, the selected sample period runs from 01/1990 to 2/2009. Following Koop (2011), we transform the data-set to make variables approximately stationary. For both, sVAR and msVAR, BIC selects the number of lags to be $p = 2$. The same number of lags $p = 2$ is used for other four sparse VAR methods.

We compare the out-of-sample forecast performance for the above six VAR methods using

the last 24 months ($T_{test} = 24$) as test data. We use the h-step-ahead forecast root mean squared error (RMSE) as a measure for the comparison.

$$\text{RMSE}(h) = \left[K^{-1}(T_{test} - h + 1)^{-1} \sum_{k=1}^{K} \sum_{t=T}^{T+T_{test}-h} (\hat{Y}_{t+h,k} - Y_{t+h,k})^2 \right]^{1/2},$$

where $\hat{Y}_{t+h,k}$ is the h-step-ahead forecast of $Y_{t+h,k}$ for $k = 1, \ldots, K$. Table 4 summarizes RMSE(h) for a forecast horizon $h = 1, 2, 3$ and 4. It can be seen that the sVAR perform slightly better than the msVAR for all $h = 1, \ldots, 4$ and HVARC is the best among six methods.

Table 4: The h-step ahead forecast root mean squared error (RMSE(h)).

	h = 1	h = 2	h = 3	h = 4
msVAR	0.179 (0.07)	0.145 (0.008)	0.151 (0.01)	0.091(0.004)
sVAR	0.149 (0.055)	0.123 (0.008)	0.131 (0.009)	0.086 (0.007)
BRRVAR	0.156 (0.004)	0.153(0.007)	0.158 (0.008)	0.149 (0.004)
LASSOVAR	0.111(0.008)	0.099(0.012)	0.088(0.018)	0.068 (0.008)
HVARC	**0.107** (0.008)	**0.086** (0.012)	**0.074** (0.018)	**0.053** (0.008)
HVAROO	0.115 (0.008)	0.097(0.011)	0.083 (0.017)	0.069(0.009)

Note: * Parentheses contain estimated Standard Deviations.

6 Conclusion

We have proposed the msVAR method, a modification of the two-stage sVAR method in Davis et al. (2016), where we substitute the first stage of the sVAR with the new and powerful time series graphical lasso algorithm to identify/estimate zeros of the inverse spectral density matrix while recognizing that its entries are complex-valued. The second stage implements refinement of the non-zero entries using FDR. This paper focuses on algorithmic and numerical results. Real data analysis and simulation results show usefulness of our method. Theoretical properties of our method, such as the consistency and the support recovery of the msVAR, are left for future research.

A   Appendix

A.1   Link Between AR coefficient and PSC

As discussed, the assertion (8) is not exact and can be violated for some AR models. Here, relying on the framework developed in Songsiri et al. (2009), we discuss the conditions when (8) is exact.

The spectral density of the VAR process can be expressed as

$$f^Y(\omega) = \mathbf{A}^{-1}(e^{i\omega})\Sigma\mathbf{A}^{-H}(e^{i\omega}),$$

where $\mathbf{A}^{-1}(z)$ is the transfer function from ω to Y, $\mathbf{A} = I + z^{-1}A_1 + \cdots + z^{-p}A_p$, B^H is the Hermitian transpose of matrix B and $i = \sqrt{-1}$. Therefore, the inverse spectrum of an AR process is a trigonometric matrix polynomial

$$\Theta^Y(\omega) = \mathbf{A}^H(e^{i\omega})\Theta\mathbf{A}(e^{i\omega}) = X_0 + \sum_{k=1}^{p}(e^{-ik\omega}X_k + e^{ik\omega}X_k^T), \tag{22}$$

where $\Theta = \Sigma^{-1}$, $X_k = \sum_{i=0}^{p-k} A_i^T\Theta A_{i+k}$ with $A_0 = I$. From (4) and (22) we obtain,

$$\text{PSC}_{ij}(\omega) = 0 \Leftrightarrow (X_k)_{ij} = 0 \text{ for } k = 0, \ldots, p. \tag{23}$$

B   Derivation of updates using Wirtinger Calculus

Before providing details on solving updates (a) and (b) for (18), we give a brief overview of Wirtinger calculus. Deeper treatment of the subject can be found in Remmert (1991); Kreutz-Delgado (2009) and in a pithy presentation by Brandwood (1983).

B.1   Wirtinger Calculus

Let $z = x + iy$, where x, y are real and $i = \sqrt{-1}$. Consider a general complex-valued function $f(z) = u(x, y) + iv(x, y)$, where we assume that the partial derivatives of u and v exist. Then the standard complex derivative $f'(z)$ exist if $f(z)$ is holomorphic or Cauchy-Riemann equations are satisfied, i.e.,

$$\frac{\partial u}{\partial v} = \frac{\partial v}{\partial y}, \ \ \frac{\partial v}{\partial x} = -\frac{\partial u}{\partial y}$$

Unfortunately, those conditions are strong, and the functions that we are usually interested in violate them. For example, $f(z) = |z|^2 = z^* z$, where z^* is the conjugate of z. However, since real partial derivatives of a non-holomorphic function exist, one can exploit the real R^2 vector space structure, which underlies C, and represent $f(z) = f(x, y) : R^2 \to R$. Remmert (1991) called the differentiation of this function R-derivative to avoid confusion with the standard complex derivative. As discussed in Kreutz-Delgado (2009, Section 3.1), this representation can not be viewed as an admissible generalization of the standard complex derivative, since it, as well, suffers from some drawbacks. For example, it does not reduce to the standard complex derivative when a function $f(z)$ is holomorphic.

The generalization, in a sense discussed above, were developed in the notion of Wirtinger calculus (Wirtinger, 1927; Brandwood, 1983). In particular, a complex function $f(z)$ is viewed as a function of z and its conjugate z^*

$$f(z) = f(z, z^*) = u(x, y) + iv(x, y).$$

It can be shown that $f(z, z^*)$ is holomorphic in z for fixed z^*, and, similarly, holomorphic in z^* for fixed z. Then the Wirtinger derivative and its conjugate are defined as

$$\frac{\partial f(z, z^*)}{\partial z}, \ \ \frac{\partial f(z, z^*)}{\partial z^*}$$

For example, for the function $f(z) = |z|^2 = z^*z$, $\frac{\partial f(z,z^*)}{\partial z} = z^*$ and $\frac{\partial f(z,z^*)}{\partial z*} = z$.

B.2   Solving Updates (a) and (b)

The derived formulas for updates (a) and (b) are given in (28) and (34), respectively. It is instructive to note that, $L_\rho(\Theta[\cdot], Z[\cdot], U[\cdot])$ is separable in n and the update of (a) can be implemented in parallel by minimizing $J(\Theta[n])$, $n = 1, \ldots, N$, where

$$J(\Theta[n]) = -\log \det(\Theta[n]) + \mathrm{tr}(\tilde{f}[n]\Theta[n]) + \rho/2\|\Theta[n] - Z^{(k)}[n] + U^{(k)}[n]\|_F^2 \qquad (24)$$

To use Wirtinger calculus, we write $J(\Theta[n]) = J(\Theta[n], \Theta^*[n])$ as a function of Θ and its complex conjugate Θ^*. Thus, (24) can be written as

$$
\begin{aligned}
J(\Theta[n], \Theta^*[n]) = -\frac{1}{2}\Big[&\log \det(\Theta[n]) + \log \det(\Theta^*[n]) + \mathrm{tr}(\tilde{f}[n]\Theta[n]) + \mathrm{tr}(\tilde{f}^*[n]\Theta^*[n]) \\
&+ \rho\,\mathrm{tr}(\Theta[n] - Z^{(k)}[n] + U^{(k)}[n])(\Theta[n] - Z^{(k)}[n] + U^{(k)}[n])^H)\Big]
\end{aligned}
\qquad (25)
$$

Then in update (a), a necessary and sufficient condition for a global optimum is that the gradient $J(\Theta[n], \Theta^*[n])$ with respect to $\Theta^*[n])$ is zero (Brandwood, 1983):

$$\Theta^{-1}[n] + \tilde{f}[n] + \rho(\Theta[n] - Z^{(k)}[n] + U^{(k)}[n]) = 0 \qquad (26)$$

The solution to (26) follows as in Boyd et al. (2011, Section 6.5). Let the eigen-decomposition of the matrix $\rho(Z^{(k)}[n] - U^{(k)}[n]) - \tilde{f}[n]$ be $V_n C_n V_n^H$. Then

$$\Theta^{(k+1)} = V_n \tilde{C}_n V_n^H, \qquad (27)$$

where $\tilde{C}_n$ is the diagonal matrix with the jth diagonal element

$$(\tilde{C}_n)_{jj} = (1/2\rho)(-(C_n)_{jj} + \sqrt{(C_n)_{jj} + 4\rho}). \qquad (28)$$

Finally, the update (a) is completed by obtaining the preceding solution for $n = 1, 2, \ldots, N$.

For an update (b), we consider the following two lemmas. The first lemma derives the Wirtinger subgradient for the penalty term in (17), and the second lemma provides an update for (b).

Lemma 1. *Given $x \in C^N$, the Wirtinger subgradient of the function $T : C^N \to R$, where $T(x) = \|x\|_2$ is*

$$\partial^W T(x) = \begin{cases} \frac{x}{2\|x\|_2}, & \text{if } x \neq 0 \\ \in \{u| \|u\|_2 \leq 1/2, \, u \in C^p\}, & \text{if } x = 0 \end{cases} \quad (29)$$

Proof. We start from the $x \neq 0$ case. The derivative of $T(x, x^*) = \|x\|_2 = (x^H x)^{1/2}$ with respect to the conjugate x^* is

$$\frac{\partial T(x)}{x^*} = \frac{x}{2\|x\|_2}$$

For the case $x = 0$, to find the subgradient $\partial^W T(x^*)$ of the function $T(x)$, we exploit Bouboulis et al. (2012, Definition 3). From which, $\partial^W T(x)$ is a Wirtinger subgradient if it satisfies

$$T(y) \geq T(x) + 2\text{Re}((y - x)^H (\partial^W T(x))^*), \, y \in C^N \quad (30)$$

where $\text{Re}(\cdot)$ indicates the real part of the complex variable. From (30), we have for $x = 0$ and any $y \in C^N$

$$\|y\|_2 \geq 2\text{Re}((y)^H (\partial^W T(x))^*) \quad (31)$$

But (31) is just the definition of the dual function of $\|x\|_2$, which is also ℓ_2 norm (Horn and Johnson, 2012), and the result follows. ∎

For the next lemma, we define the generic function $h : C^N \to R$

$$h(x) = \frac{1}{2}\|a - x\|_2^2 + \lambda\|x\|_2 \quad (32)$$

and denote by $\hat{x} = \arg\min_x h(x)$.

Lemma 2. *The ith component of the global minimum of $h(x)$ has the following closed form solution*

$$\hat{x}_i = S_{\lambda/\rho}(a_i), \tag{33}$$

where $S_\mu(a_i) = (1 - \mu/\|a\|_2)a_i$

Proof. The proof of the lemma relies on the framework developed in Friedman et al. (2010), Lemma 1 and Wirtinger calculus. Since $h(x)$ is convex on x, a necessary and sufficient condition for a global minimum x^* is that the Wirtinger subdifferntial $\partial^W h(x) \in 0$. Thus, we solve

$$0 \in \frac{1}{2}(x - a) + \gamma,$$

where γ is a subgradient from Lemma 1. Then, the result can be derived following steps as in Friedman et al. (2010, Section 2).

∎

Invoking the Lemma 2, the update (b) for $i \neq j$ is

$$Z_{ij}^{(k+1)}[n] = S_{\lambda/\rho}(\Theta_{ij}^{(k+1)}[n] + U_{ij}^{(k)}[n]) \tag{34}$$

and $Z_{ij}^{(k+1)}[n] = \Theta_{ii}^{(k+1)}[n]$ for $i = j$, since we do not penalize diagonal elements.

References

Banbura, M., D. Giannone, and L. Reichlin (2010), "Large bayesian vars." *Journal of Applied Econometrics*, 25, 71–92.

Banerjee, Onureena, Laurent El Ghaoui, and Alexandre d'Aspremont (2008), "Model selection through sparse maximum likelihood estimation for multivariate gaussian or binary data." *J. Mach. Learn. Res.*, 9, 485–516.

Barber, RF and E. Candès (2015), "Controlling the false discovery rate via knockoffs." *The Annals of Statistics*, 43, 2055–2085.

Barigozzi, Matteo and Christian Brownlees (2019), "Nets: Network estimation for time series." *Journal of Applied Econometrics*, 34, 347–364.

Basu, Sumanta and George Michailidis (2015), "Regularized estimation in sparse high-dimensional time series models." *Ann. Statist.*, 43, 1535–1567.

Benjamini, Y and Y. Gavrilov (2009), "A simple forward selection procedure based on false discovery rate control." *The Annals of Applied Statistics*, 3, 179–198.

Benjamini, Y and Y. Hochberg (1995), "Controlling the false discovery rate: a practical and powerful approach to multiple testing." *Journal of the royal statistical society. Series B*, 289–300.

Bouboulis, P., K. Slavakis, and S. Theodoridis (2012), "Adaptive learning in complex reproducing kernel hilbert spaces employing wirtinger's subgradients." *IEEE Transactions on Neural Networks and Learning Systems*, 23, 425–438.

Boyd, Stephen, Neal Parikh, Eric Chu, Borja Peleato, and Jonathan Eckstein (2011), "Distributed optimization and statistical learning via the alternating direction method of multipliers." *Found. Trends Mach. Learn.*, 3, 1–122.

Brandwood, D. H. (1983), "A complex gradient operator and its application in adaptive array theory." *IEE Proceedings F - Communications, Radar and Signal Processing*, 130, 11–16.

Brillinger, David R. (1981), *Time Series: Data Analysis and Theory*. Society for Industrial and Applied Mathematics, Philadelphia, PA, USA.

Brillinger, David R. (1996), "Remarks concerning graphical models for time series and point processes." *Brazilian Review of Econometrics*, 16.

Brockwell, Peter J and Richard A Davis (1986), *Time Series: Theory and Methods*. Springer-Verlag New York, Inc., New York, NY, USA.

Dahlhaus, Rainer (2000), "Graphical interaction models for multivariate time series." *Metrika*, 51, 157–172.

Danaher, Patrick, Pei Wang, and Daniela M Witten (2014), "The joint graphical lasso for inverse covariance estimation across multiple classes." *Journal of the Royal Statistical Society: Series B (Statistical Methodology)*, 76, 373–397.

Davis, Richard A., Pengfei Zang, and Tian Zheng (2016), "Sparse vector autoregressive modeling." *Journal of Computational and Graphical Statistics*, 25, 1077–1096.

Ding, Xin, Ziyi Qiu, and Xiaohui Chen (2017), "Sparse transition matrix estimation for high-dimensional and locally stationary vector autoregressive models." *Electron. J. Statist.*, 11, 3871–3902.

Eichler, M. (2012), "Graphical modelling of multivariate time series." *Probab. Theory Related Fields*, 153, 233–268.

Foti, N., Rahul Nadkarni, A. Lee, and E. Fox (2016), "Sparse plus low-rank graphical models of time series for functional connectivity in meg." In *2nd SIGKDD Workshop on Mining and Learning from Time Series*.

Foygel, Rina and Mathias Drton (2010), "Extended bayesian information criteria for gaussian graphical models." In *Proceedings of the 23rd International Conference on Neural Information Processing Systems - Volume 1*, NIPS'10, 604–612, Curran Associates Inc.

Friedman, J, T Hastie, and R. Tibshirani (2008), "Sparse inverse covariance estimation with the graphical lasso." *Biostatistics*, 9, 432–441.

Friedman, Jerome H., Trevor J. Hastie, and Robert Tibshirani (2010), "A note on the group lasso and a sparse group lasso."

G'Sell, MG, S Wager, A Chouldechova, and R. Tibshirani (2016), "Sequential selection procedures and false discovery rate control." *Journal of the royal statistical society: series B*, 78, 423–444.

Guo, Jian, Elizaveta Levina, George Michailidis, and Ji Zhu (2011), "Joint estimation of multiple graphical models." *Biometrika*, 98, 1–15.

Han, Fang, Huanran Lu, and Han Liu (2015), "A direct estimation of high dimensional stationary vector autoregressions." *Journal of Machine Learning Research*, 16, 3115–3150.

Homrighausen, Darren and J. Daniel McDonald (2018), "A study on tuning parameter selection for the high-dimensional lasso." *Journal of Statistical Computation and Simulation*, 88, 2865–2892.

Horn, Roger A. and Charles R. Johnson (2012), *Matrix Analysis*, 2nd edition. Cambridge University Press, New York, NY, USA.

Jung, Alexander, Gabor Hannak, and Norbert Goertz (2015), "Graphical lasso based model selection for time series." *IEEE Signal Processing Letters*, 22, 1781–1785.

Kock, Anders and Laurent Callot (2015), "Oracle inequalities for high dimensional vector autoregressions." *Journal of Econometrics*, 186, 325–344.

Koop, Gary M (2011), "Forecasting with medium and large bayesian vars." *Journal of Applied Econometrics*, 28, 177–203.

Kreutz-Delgado, Ken (2009), "The complex gradient operator and the cr-calculus."

Li, Lu, XingyuWang, and GuoqiangWang (2015), "Alternating direction method of multipliers for separable convex optimization of real functions in complex variables." *Mathematical Problems in Engineering*, 2015.

Lütkepohl, Helmut (2007), *New Introduction to Multiple Time Series Analysis*. Springer, New York.

Meinshausen, Nicolai and Peter Bühlmann (2010), "Stability selection." *Journal of the Royal Statistical Society: Series B (Statistical Methodology)*, 72, 417–473.

Nicholson, William B., Jacob Bien, and David S. Matteson (2016), "Hierarchical vector autoregression." *Arxiv preprint arXiv:1412.5250v2*.

Pourahmadi, Mohsen (2013), *High-Dimensional Covariance Estimation*. John Wiley & Sons, Ltd.

Remmert, Reinhold (1991), *Theory of Complex Functions*. Springer, New York.

Safikhani, Abolfazl and Ali Shojaie (2020), "Joint structural break detection and parameter estimation in high-dimensional nonstationary var models." *Journal of the American Statistical Association*, 0, 1–14.

Song, S. and P. J. Bickel (2011), "Large vector auto regressions." *Arxiv preprint arXiv:1106.3915*.

Songsiri, Jitkomut, Joachim Dahl, and Lieven Vandenberghe (2009), *Graphical models of autoregressive processes*, 89–116. Cambridge University Press.

Stock, James and Mark Watson (2005), "An empirical comparison of methods for forecasting using many predictors." *Manuscript, Princton University.*

Stoica, P. and R.L. Moses (1997), *Introduction to Spectral Analysis.* Prentice Hall.

Tugnait, J. K. (2018), "Graphical modeling of high-dimensional time series." In *2018 52nd Asilomar Conference on Signals, Systems, and Computers*, 840–844.

Whittaker, J. (1990), *Graphical models in applied multivariate statistics.* John Wiley & Sons, Ltd.

Wirtinger, W. (1927), "Zur formalen theorie der funktionen von mehr komplexen veränderlichen." *Mathematische Annalen*, 97, 357–375.

Wu, Wei-Biao and Ying Nian Wu (2016), "Performance bounds for parameter estimates of high-dimensional linear models with correlated errors." *Electron. J. Statist.*, 10, 352–379.

Yuen, T.P., H. Wong, and K.F.C. Yiu (2018), "On constrained estimation of graphical time series models." *Computational Statistics and Data Analysis*, 124, 27 – 52.